

# A Review of Nonparametric Hypothesis Tests of Isotropy Properties in Spatial Data

Zachary D. Weller and Jennifer A. Hoeting

Department of Statistics, Colorado State University

*Abstract.* An important aspect of modeling spatially-referenced data is appropriately specifying the covariance function of the random field. A practitioner working with spatial data is presented a number of choices regarding the structure of the dependence between observations. One of these choices is determining whether or not an isotropic covariance function is appropriate. Isotropy implies that spatial dependence does not depend on the direction of the spatial separation between sampling locations. Misspecification of isotropy properties (directional dependence) can lead to misleading inferences, e.g., inaccurate predictions and parameter estimates. A researcher may use graphical diagnostics, such as directional sample variograms, to decide whether the assumption of isotropy is reasonable. These graphical techniques can be difficult to assess, open to subjective interpretations, and misleading. Hypothesis tests of the assumption of isotropy may be more desirable. To this end, a number of tests of directional dependence have been developed using both the spatial and spectral representations of random fields. We provide an overview of nonparametric methods available to test the hypotheses of isotropy and symmetry in spatial data. We summarize test properties, discuss important considerations and recommendations in choosing and implementing a test, compare several of the methods via a simulation study, and propose a number of open research questions. Several of the reviewed methods can be implemented in R using our package `spTest`, available on CRAN.

*MSC 2010 subject classifications:* Primary 62M30, ; secondary 62G10.

*Key words and phrases:* isotropy, symmetry, nonparametric spatial covariance.

## 1. INTRODUCTION

Early spatial models relied on the simplifying assumptions that the covariance function is stationary and isotropic. With the emergence of new sources of spatial

(e-mail: [wellerz@stat.colostate.edu](mailto:wellerz@stat.colostate.edu)) (e-mail: [jah@stat.colostate.edu](mailto:jah@stat.colostate.edu))

\*Weller's work was supported by the National Science Foundation Research Network on Statistics in the Atmospheric and Ocean Sciences (STATMOS) (DMS-1106862). Hoeting's research was supported by the National Science Foundation (AGS-1419558).

<sup>†</sup>The authors would like to thank Peter Guttorp and Alexandra Schmidt for organizing the Pan-American Advanced Study Institute (PASI) on spatiotemporal statistics in June 2014 which inspired this work.

data, for instance, remote sensing via satellite, climate model output, or environmental monitoring, a variety of methods and models have been developed that relax these assumptions. In the case of anisotropy, there are a number of methods for modeling both zonal anisotropy (Journel and Huijbregts, 1978, pg. 179-184; Ecker and Gelfand, 2003; Schabenberger and Gotway, 2004, pg. 152; Banerjee et al., 2014, pg. 31) and geometric anisotropy (Borgman and Chao, 1994; Ecker and Gelfand, 1999). Rapid growth of computing power has allowed the implementation and estimation of these models.

When modeling a spatial process, the specification of the covariance function will have an effect on kriging and parameter estimates and the associated uncertainty (Cressie, 1993, pg. 127-135). Sherman (2011, pg. 87-90) and Guan et al. (2004) use numerical examples to demonstrate the adverse implications of incorrectly specifying isotropy properties on kriging estimates. Given the variety of choices available regarding the properties of the covariance function (e.g., parametric forms, isotropy, stationarity) and the effect these choices can have on inference, practitioners may seek methods to inform the selection of an appropriate covariance model.

A number of graphical diagnostics have been proposed to determine isotropy properties. Perhaps the most commonly used methods are directional semivariograms and rose diagrams (Matheron, 1961; Isaaks and Srivastava, 1989, pg. 149-154). Banerjee et al. (2014, pg. 38-40) suggest using an empirical semivariogram contour plot to assess isotropy as a more informative method than directional sample semivariograms. Another technique involves comparing empirical estimates of the covariance at different directional lags to assess symmetry for data on gridded sampling locations (Modjeska and Rawlings, 1983). One caveat of the aforementioned methods is that they can be challenging to assess, are open to subjective interpretations, and can be misleading (Guan et al., 2004) because they typically do not include a measure of uncertainty. Experienced statisticians may have intuition about the interpretation and reliability of these diagnostics, but a novice user may wish to evaluate assumptions via a hypothesis test.

Statistical hypothesis tests of second order properties can be used to supplement and reinforce intuition about graphical diagnostics and can be more objective. Like the graphical techniques, hypothesis tests have their own caveats; for example, a parametric test of isotropy demands specification of the covariance function. A nonparametric method for testing isotropy avoids the potential problems of misspecification of the covariance function and the requirement of model estimation under both the null and alternative hypothesis, which can be computationally expensive for large datasets. Furthermore, nonparametric methods do not require the common assumption of geometric anisotropy. However, in abandoning the parametric assumptions about the covariance function, implementing a test of isotropy presents several challenges (see Section 5). A nonparametric test of isotropy or symmetry can serve as another form of exploratory data analysis that supplements graphical techniques and informs the choice of an appropriate nonparametric or parametric model. Figure 1 illustrates the process for assessing and modeling isotropy properties.

In this article we review nonparametric hypothesis tests developed to test the assumptions of symmetry and isotropy in spatial processes. We summarize tests in both the spatial and spectral domain and provide tables that enable convenient

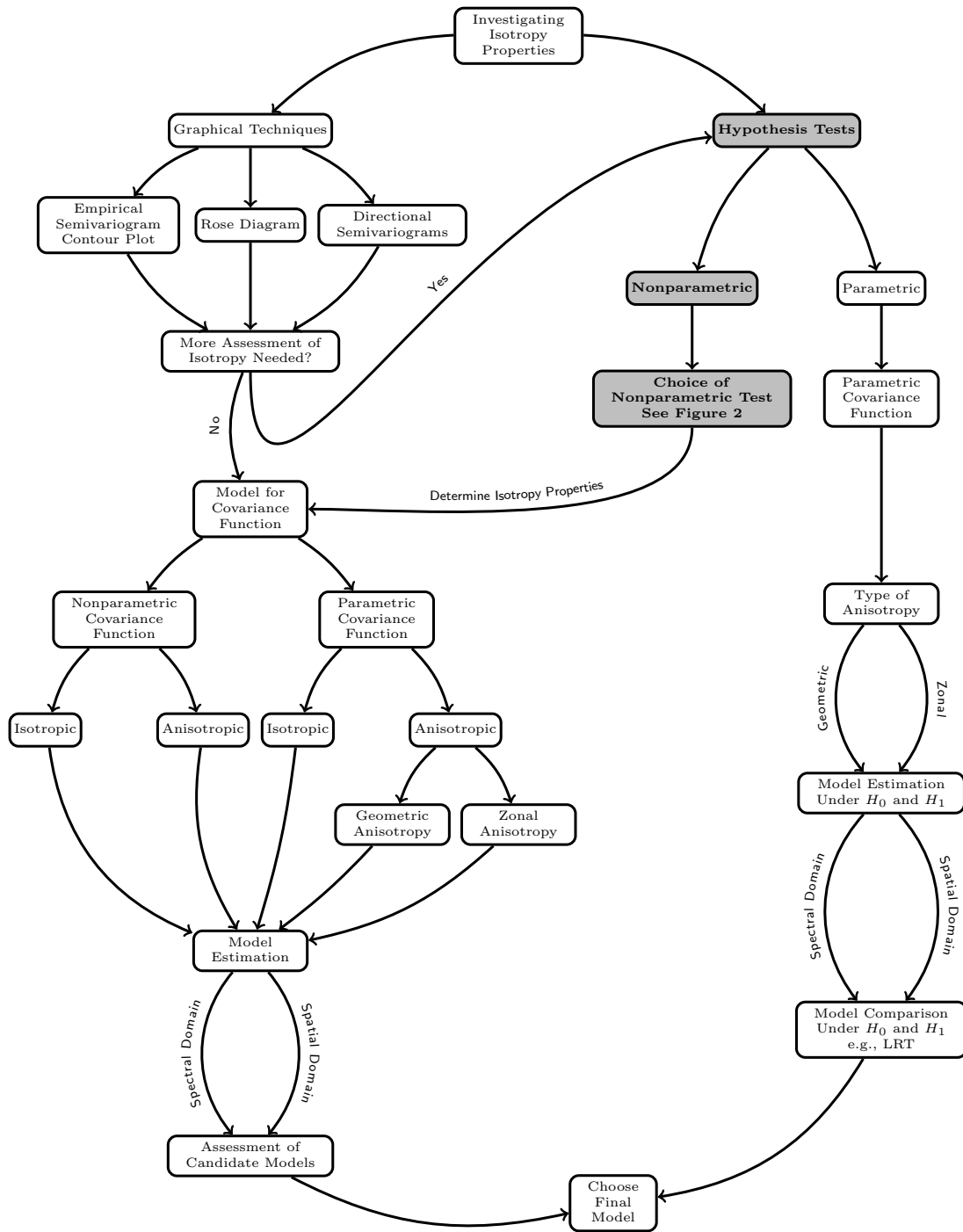


Fig 1: A flow chart illustrating the process of determining and modeling isotropy in spatial data. The gray boxes indicate the focus of this paper.

comparisons of test properties. A simulation study evaluates the empirical size and power of several of the methods and enables a direct comparison of method performance. The simulations also lead to new insights into test performance and implementation beyond those given in the original works. Finally, we include graphics that demonstrate considerations for choosing a nonparametric test and illustrate the process of determining isotropy properties.

The remainder of this article is organized as follows: Section 2 establishes notation and definitions; Section 3 details the various nonparametric hypothesis tests of isotropy and symmetry and includes Tables 1-3 which facilitate comparison between tests as well as test selection for users; Section 4 describes the simulation study comparing the various methods; Sections 5 and 6 provide discussion and conclusions. Additional details on the simulation study are specified in the Appendix.

## 2. NOTATION AND DEFINITIONS

Here we briefly review key definitions required for tests of isotropy. For additional background, see [Schabenberger and Gotway \(2004\)](#). Let  $\{Y(\mathbf{s}) : \mathbf{s} \in \mathcal{D} \subseteq \mathbb{R}^d, d > 1\}$  be a second order stationary random field (RF). Below we will assume that  $d = 2$ , although many of the results hold for the more general case of  $d > 2$ . For a spatial lag  $\mathbf{h} = (h_1, h_2)$ , the semivariogram function describes dependence between observations,  $Y$ , at spatial locations separated by lag  $\mathbf{h}$  and is defined as

$$(2.1) \quad \gamma(\mathbf{h}) = \frac{1}{2} \text{Var}(Y(\mathbf{s} + \mathbf{h}) - Y(\mathbf{s})).$$

The classical, moment-based estimator of the semivariogram ([Matheron, 1962](#)) is

$$(2.2) \quad \hat{\gamma}(\mathbf{h}) = \frac{1}{2|\mathcal{D}(\mathbf{h})|} \sum [Y(\mathbf{s}) - Y(\mathbf{s} + \mathbf{h})]^2,$$

where the sum is over  $\mathcal{D}(\mathbf{h}) = \{\mathbf{s} : \mathbf{s}, \mathbf{s} + \mathbf{h} \in \mathcal{D}\}$  and  $|\mathcal{D}(\mathbf{h})|$  is the number of elements in  $\mathcal{D}(\mathbf{h})$ . The set  $\mathcal{D}(\mathbf{h})$  is the set of sampling location pairs that are separated by spatial lag  $\mathbf{h}$ . The covariance function,  $C(\mathbf{h})$ , is an alternative to the semivariogram for describing spatial dependence and is given by  $C(\mathbf{h}) = \lim_{\|\mathbf{v}\| \rightarrow \infty} \gamma(\mathbf{v}) - \gamma(\mathbf{h})$  if the limit exists.

Let  $\{\mathbf{s}_1, \dots, \mathbf{s}_n\} \subset \mathcal{D}$  be the finite set of locations at which the random process is observed, providing the random vector  $(Y(\mathbf{s}_1), \dots, Y(\mathbf{s}_n))^T$ . The sampling locations may follow one of several spatial sampling designs: gridded locations, randomly and uniformly distributed locations, or a cluster design. Some authors make the distinction between a lattice process and a geostatistical process observed on a grid ([Fuentes and Reich, 2010](#); [Schabenberger and Gotway, 2004](#), pg. 6-10). We do not explore this distinction further and will use the term grid throughout.

It is often of interest to infer the effect of covariates on the process, deduce dependence structure, and/or predict  $Y$  with quantifiable uncertainty at new locations. To achieve these goals, the practitioner must specify the distributional properties of the spatial process. A common assumption is that the finite-dimensional joint distribution is multivariate normal (MVN), in which case we call the RF

a Gaussian random field (GRF). We are interested in second order properties; thus, hereafter we assume that the mean of the RF is zero.

A common simplifying assumption on the spatial dependence structure is that it is isotropic.

**DEFINITION 2.1.** *A second order stationary spatial process is isotropic if the semivariogram,  $\gamma(\mathbf{h})$ , [or equivalently, the covariance function  $C(\mathbf{h})$ ] of the spatial process depends on the lag vector  $\mathbf{h}$  only through its Euclidean length,  $h = \|\mathbf{h}\|$ , i.e.,  $\gamma(\mathbf{h}) = \gamma_0(h)$  for some function  $\gamma_0(\cdot)$  of a univariate argument.*

Isotropy implies that the dependence between any two observations depends only on the distance between their sampling locations and not on their relative orientation. A spatial process that is not isotropic is called anisotropic. Anisotropy is broadly categorized as either geometric or zonal (Zimmerman, 1993). In practice, if a process is assumed to be anisotropic, it is usually assumed to be geometrically anisotropic due to its precise formal and functional definition (Ecker and Gelfand, 1999). Geometric anisotropy is governed by a scaling parameter,  $R$ , and rotation parameter,  $\theta$ , and implies the anisotropy can be corrected via a linear transformation of the lag vector or, equivalently, the sampling locations (Cressie, 1993, pg. 64).

Symmetry is another directional property of the covariance (semivariogram) function, which is often used to describe the spatial variation of processes on a grid. We discuss symmetry properties here as they are a subset of isotropy, and methods for testing isotropy can often be used to test symmetry. The following definitions come from Lu and Zimmerman (2005) and Scaccia and Martin (2005) where the notation  $C(h_1, h_2)$  denotes the covariance between random variables located  $h_1$  columns and  $h_2$  rows apart on a rectangular grid, denoted  $\mathcal{L}^2$ .

**DEFINITION 2.2.** *A second order stationary spatial process on a grid is reflection or axially symmetric if  $C(h_1, h_2) = C(-h_1, h_2)$  for all  $(h_1, h_2) \in \mathcal{L}^2$ .*

**DEFINITION 2.3.** *A second order stationary spatial process on a grid is diagonally or laterally symmetric if  $C(h_1, h_2) = C(h_2, h_1)$  for all  $(h_1, h_2) \in \mathcal{L}^2$ .*

**DEFINITION 2.4.** *A second order stationary spatial process on a grid is completely symmetric if it is both reflection and laterally symmetric, i.e.,  $C(h_1, h_2) = C(-h_1, h_2) = C(h_2, h_1) = C(-h_2, h_1)$  for all  $(h_1, h_2) \in \mathcal{L}^2$ .*

Complete symmetry is a weaker property than isotropy. Isotropy requires that  $C(h_1, h_2)$  depends only on  $\sqrt{h_1^2 + h_2^2}$  for all  $h_1, h_2$ . The relationship between these properties is given by:

$$(2.3) \quad \text{isotropy} \implies \text{complete symmetry} \implies \begin{matrix} \text{reflection symmetry} \\ \text{diagonal symmetry} \end{matrix}.$$

Thus, rejecting a null hypothesis of reflection symmetry implies evidence against the assumptions of reflection symmetry, complete symmetry, and isotropy. However, failure to reject a null hypothesis of reflection symmetry does not imply an assumption of complete symmetry or isotropy is appropriate.

The aforementioned properties of isotropy and symmetry were defined in terms of examining the spatial random process in the spatial domain, where second order properties depend on the spatial separation,  $\mathbf{h}$ . Alternatively, a spatial random process can be represented in the spectral domain using Fourier analysis. For the purposes of investigating second order properties, we are interested in the spectral representation of the covariance function, called the spectral density function and denoted  $f(\boldsymbol{\omega})$ , where  $\boldsymbol{\omega} = (\omega_1, \omega_2)$ . Under certain conditions and assumptions (Fuentes and Reich, 2010, pg. 62), the spectral density function is given by

$$(2.4) \quad f(\boldsymbol{\omega}) = \frac{1}{(2\pi)^2} \int_{\mathbb{R}^2} \exp(-i\boldsymbol{\omega}^T \mathbf{h}) C(\mathbf{h}) d\mathbf{h},$$

so that the covariance function,  $C(\mathbf{h})$ , and the spectral density function,  $f(\boldsymbol{\omega})$ , form a Fourier transform pair.

Properties of the covariance function imply properties of the spectral density. For example, if the covariance function is isotropic (2.1), then the spectral density (2.4) depends on  $\boldsymbol{\omega}$  only through its length,  $\omega = \|\boldsymbol{\omega}\|$ , and we can write  $f(\boldsymbol{\omega}) = f_0(\omega)$ , where  $f_0(\cdot)$  is called the isotropic spectral density (Fuentes, 2013). Consequently, second order properties of a second order stationary RF can be explored via either the covariance function or the spectral density function. Test statistics quantifying second order properties can be constructed using the periodogram, an estimator of (2.4) and denoted by  $I(\cdot)$ . For a real-valued spatial process on a rectangular grid  $\mathbb{Z}^2 \subset \mathbb{R}^2$ , a moment-based periodogram used to estimate (2.4) is

$$(2.5) \quad I(\omega_1, \omega_2) = \frac{1}{(2\pi)^2} \sum_{h_1=-n_1+1}^{n_1-1} \sum_{h_2=-n_2+1}^{n_2-1} \hat{C}(h_1, h_2) \cos(h_1\omega_1 + h_2\omega_2),$$

where  $n_1$  and  $n_2$  denote the number of rows and columns of the grid and  $\hat{C}(h_1, h_2)$  is a non-parametric estimator of the covariance function. In practice, the periodogram (2.5) is used to estimate the spectral density at the Fourier or harmonic frequencies. The frequency  $\boldsymbol{\omega} = (\omega_1, \omega_2)$  is a Fourier or harmonic frequency if  $\omega_j$  is a multiple of  $2\pi/n_j$ ,  $j = 1, 2$ . Furthermore, the set of frequencies is limited to  $\{\omega_j = 2\pi k_j/n_j, k_j = 1, 2, \dots, n_j^*\}$ , where  $n_j^*$  is  $(n_j - 1)/2$  if  $n_j$  is odd and  $n_j/2 - 1$  if  $n_j$  is even.

### 3. TESTS OF ISOTROPY AND SYMMETRY

#### 3.1 Brief History

Matheron (1961) developed one of the earliest hypothesis test of isotropy when he used normality of sample variogram estimators to construct a  $\chi^2$  test for anisotropy in mineral deposit data. Cabana (1987) tested for geometric anisotropy using level curves of random fields. Vecchia (1988) and Baczkowski and Mardia (1990) developed tests for isotropy assuming a parametric covariance function. Baczkowski (1990) also proposed a randomization test for isotropy. Despite these early works, little work on testing isotropy was published during the 1990s, although the PhD dissertation work of Lu (1994) would eventually have a noteworthy impact on the literature. Then, in the 2000s, a number of nonparametric tests

of second-order properties emerged. Some of the developments used estimates of the variogram or covariogram to test symmetry and isotropy properties (Lu and Zimmerman, 2001; Guan, 2003; Guan et al., 2004, 2007; Maity and Sherman, 2012). These works generally borrowed ideas from two bodies of literature: (a) theory on the distributional and asymptotic properties of semivariogram estimators (e.g., Baczkowski and Mardia, 1987; Cressie, 1993, pg. 69-47; Hall and Patil, 1994) and (b) subsampling techniques to estimate the variance of statistics derived from spatial data (e.g., Possolo, 1991; Politis and Sherman, 2001; Sherman, 1996; Lahiri, 2003; Lahiri and Zhu, 2006). Other nonparametric methods used the spectral domain to test isotropy and symmetry (Scaccia and Martin, 2002, 2005; Lu and Zimmerman, 2005; Fuentes, 2005). These works generally extended ideas used in the time series literature (e.g., Priestley and Rao, 1969; Priestley, 1981) to the spatial case. Methods for testing isotropy and symmetry in both the spatial and spectral domains, under the assumption of a parametric covariance function, have also been developed recently (Stein et al., 2004; Haskard, 2007; Fuentes, 2007; Matsuda and Yajima, 2009; Scaccia and Martin, 2011).

### 3.2 Nonparametric Methods in the Spatial Domain

A popular approach to testing second order properties was pioneered in the works of Lu (1994) and Lu and Zimmerman (2001) who leveraged the asymptotic joint normality of the sample variogram computed at different spatial lags. The subsequent works of Guan et al. (2004, 2007) and Maity and Sherman (2012) built upon these ideas and are the primary focus of this subsection. Lu (1994) details methods for testing axial symmetry. While Lu and Zimmerman (2001), Guan et al. (2004), and Maity and Sherman (2012) focus on testing isotropy, these methods can also be used to test symmetry. Finally, Bowman and Crujeiras (2013) detail a more computational approach for testing isotropy. Both Li et al. (2007, 2008b) and Jun and Genton (2012) use an approach analogous to the methods from Lu and Zimmerman (2001), Guan et al. (2004, 2007), and Maity and Sherman (2012) but for spatiotemporal data. Table 1 summarizes test properties discussed in this section and Section 3.3.

Nonparametric tests for anisotropy in the spatial domain are based on a null hypothesis that is an approximation to isotropy. Under the null hypothesis that the RF is isotropic, it follows that the values of  $\gamma(\cdot)$  evaluated at any two spatial lags that have the same norm are equal, regardless of the direction of the lags. To fully specify the most general null hypothesis of isotropy, theoretically, one would need to compare variogram values for an infinite set of lags. In practice a small number of lags are specified. Then it is possible to test a hypothesis consisting of a set of linear contrasts of the form

$$(3.1) \quad H_0 : \mathbf{A}\gamma(\cdot) = \mathbf{0}$$

as a proxy for the null hypothesis of isotropy, where  $\mathbf{A}$  is a full row rank matrix (Lu and Zimmerman, 2001). For example, a set of lags, denoted  $\mathbf{\Lambda}$ , commonly used in practice for gridded sampling locations with unit spacing is

$$(3.2) \quad \mathbf{\Lambda} = \{\mathbf{h}_1 = (1, 0), \mathbf{h}_2 = (0, 1), \mathbf{h}_3 = (1, 1), \mathbf{h}_4 = (-1, 1)\},$$

and the corresponding  $\mathbf{A}$  matrix under  $H_0 : \mathbf{A}\gamma(\mathbf{\Lambda}) = \mathbf{0}$  is

$$(3.3) \quad \mathbf{A} = \begin{bmatrix} 1 & -1 & 0 & 0 \\ 0 & 0 & 1 & -1 \end{bmatrix}.$$



One of the first steps in detecting potential anisotropy is the choice of lags, as the test results will only hold for the particular set of lags considered (Guan et al., 2004). While this choice is subjective, there are several considerations and useful guidelines for determining the set of lags (see Section 5).

For nonparametric tests of symmetry, the null hypothesis of symmetry using (3.1) can be expressed by a countable set of contrasts for a process observed on a grid. Tests of symmetry will be subject to similar practical considerations as tests of isotropy, and practitioners testing symmetry properties will need to choose a small set of lags and form a hypothesis that is a surrogate for symmetry. For example, testing reflection symmetry of a process observed on the integer grid would require comparing estimates of  $C(\cdot)$  evaluated at the lag pairs  $\{(1, 0), (-1, 0)\}$ ,  $\{(2, 0), (-2, 0)\}$ ,  $\{(1, 1), (-1, 1)\}$ , etc.

The tests in Lu and Zimmerman (2001), Guan et al. (2004, 2007), and Maity and Sherman (2012) involve estimating either the semivariogram,  $\gamma(\cdot)$ , or covariance,  $C(\cdot)$ , function at the set of chosen lags,  $\mathbf{A}$ . Denoting the set of point estimates of the semivariogram/covariance function at the given lags as  $\hat{\mathbf{G}}_n$ , the true values as  $\mathbf{G}$ , and normalizing constant  $a_n$ , a central result for all three methods is that

$$(3.4) \quad a_n(\hat{\mathbf{G}}_n - \mathbf{G}) \xrightarrow[n \rightarrow \infty]{d} MVN(\mathbf{0}, \mathbf{\Sigma}),$$

under increasing domain asymptotics and mild moment and mixing conditions on the RF. Using the  $\mathbf{A}$  matrix, an estimate of the variance covariance matrix,  $\hat{\mathbf{\Sigma}}$ , and  $\hat{\mathbf{G}}_n$ , a quadratic form is constructed, and a p-value can be obtained from an asymptotic  $\chi^2$  distribution with degrees of freedom given by the row rank of  $\mathbf{A}$ . The primary differences between these works are the assumed distribution of sampling locations, the shape of the sampling domain, and the estimation of  $\mathbf{G}$  and  $\mathbf{\Sigma}$ . These differences are important when choosing a test that is appropriate for a particular set of data (see Tables 1 and 2 and Figure 4 for more information about these differences).

Maity and Sherman (2012) develop a test with the fewest restrictions on the shape of the sampling region and distribution of sampling locations. Their test can be used when the sampling region is any convex subset in  $\mathbb{R}^d$  and the distribution of sampling locations in the region follows any general spatial sampling design. The test in Guan et al. (2004) also allows convex subsets in  $\mathbb{R}^d$  and is developed for gridded and non-gridded sampling locations but requires non-gridded sampling locations to be uniformly distributed on the domain, i.e., generated by a homogenous Poisson process. The Poisson assumption is dropped in Guan et al. (2007). Lu and Zimmerman (2001) require the domain to be rectangular and the observations to lie on a grid.

Another difference between methods is the form of the nonparametric estimator of  $\mathbf{G}$ . In Lu and Zimmerman (2001),  $\hat{\mathbf{G}}_n$  is computed using the log of the classical sample semivariogram estimator (2.2). Guan et al. (2004, 2007) also use the estimator in (2.2) for gridded sampling locations, but use a kernel estimator of  $\gamma(\mathbf{h})$  for non-gridded locations. Maity and Sherman (2012) use a kernel estimator of the covariance function. When smoothing over spatial lags in  $\mathbb{R}^2$ , the kernel is typically given as Nadaraya-Watson (Nadaraya, 1964; Watson, 1964) product kernel, independently smoothing over horizontal and vertical lags. Common choices for the kernel are the Epanechnikov or truncated Gaussian kernels. The



Table 1: Properties of nonparametric tests of isotropy. “Domain” refers to the domain used to represent the RF (spatial or spectral), “Test Stat Based On” lists the nonparametric estimator used to construct the test statistic “Distb’n” gives the limiting asymptotic distribution of the test statistic, and “GP” denotes whether the test requires data to be generated from a Gaussian process.

Test Method	Hypothesis Test Properties						
	Isotropy	Symmetry	Domain	Test Stat Based On	Asymptotics	Distb’n	GP
Lu and Zimmerman (2001)	yes	yes	spatial	semivariogram	inc domain	$\chi^2$	yes
Guan et al. (2004, 2007)	yes	yes	spatial	(kernel) <sup>a</sup> variogram	inc domain	$\chi^2$ <sup>b</sup>	no
Scaccia and Martin (2002, 2005)	partial	yes	spectral	periodogram	inc domain	$Z, t$	no
Lu and Zimmerman (2005)	partial	yes	spectral	periodogram	inc domain	$\chi^2, F$	no
Fuentes (2005)	partial	no	spectral	spatial periodogram	shrinking (mixed)	$\chi^2$	yes
Maity and Sherman (2012)	yes	yes	spatial	kernel covariogram	inc domain	$\chi^2$	no
Bowman and Crujeiras (2013)	yes	no	spatial	variogram	inc domain	approx $\chi^2$	yes
Van Hala et al. (2014)	yes	yes	spectral	empirical likelihood	shrinking (mixed)	$\chi^2$	no

<sup>a</sup>for gridded sampling locations, the estimator in (2.2) is used while a kernel variogram estimator is used for non-gridded sampling locations

<sup>b</sup>p-values may need to be approximated using finite sample adjustments

Table 2: Test implementation, part 1. “Subsamp” defines whether spatial subsampling procedures are needed to perform the test, “S&P sim” denotes whether or not the author(s) of the method provide a simulation of test size and power (See also Table 3).

Test Method	Hypothesis Test Implementation				
	Sampling Domain Shape	Sampling Design	Subsamp	S&P Sim	Software
Lu and Zimmerman (2001)	rectangular in $\mathbb{R}^2$	grid	no	yes <sup>a</sup>	no
Guan et al. (2004, 2007)	convex subsets in $\mathbb{R}^d$	grid/unif <sup>b</sup> /non-unif <sup>c</sup>	yes	yes <sup>a</sup>	R package spTest
Scaccia and Martin (2002, 2005)	rectangular in $\mathbb{R}^2$	grid	no	yes <sup>a</sup>	no
Lu and Zimmerman (2005)	rectangular in $\mathbb{R}^2$	grid	no	yes	R package spTest
Fuentes (2005)	rectangular in $\mathbb{R}^d$	grid	no	yes <sup>a</sup>	no
Maity and Sherman (2012)	convex subsets in $\mathbb{R}^d$	non-unif <sup>c</sup>	yes	yes <sup>a</sup>	R package spTest
Bowman and Crujeiras (2013)	convex subsets in $\mathbb{R}^d$	unif <sup>b</sup>	no	yes <sup>a</sup>	R package sm
Van Hala et al. (2014)	subsets in $\mathbb{R}^d$	non-unif <sup>c</sup>	no	yes <sup>a</sup>	no

<sup>a</sup> simulated data are Gaussian only

<sup>b</sup> sampling locations must be generated by homogeneous Poisson process, i.e. uniformly distributed on the domain

<sup>c</sup> sampling locations can be generated by any general sampling design

kernel estimators also require the choice of a bandwidth parameter,  $w$ . Choosing an appropriate bandwidth is one of the challenges of implementing the tests for non-gridded sampling locations, and the conclusion of the test has the potential to be sensitive to the choice of the bandwidth parameter (see Section 5 for recommendations on bandwidth selection).

Nonparametric tests in the spatial domain also vary in the estimation of  $\Sigma$ , the asymptotic variance-covariance of  $\hat{\mathbf{G}}_n$  in (3.4). [Lu and Zimmerman \(2001\)](#) use a plug-in estimator, which requires the choice of a parameter,  $m$ , that truncates the sum used in estimation. Spatial resampling methods are another approach used to estimate  $\Sigma$ . The method used for spatial resampling and properties of estimators computed from spatial resampling will depend on the underlying spatial sampling design ([Lahiri, 2003](#), pg. 281). [Guan et al. \(2004, 2007\)](#) use a moving window approach, creating overlapping subblocks that cover the sampling region. [Maity and Sherman \(2012\)](#) employ the grid based block bootstrap (GBBB) ([Lahiri and Zhu, 2006](#)). The GBBB approach divides the spatial domain into regions, then replaces each region by sampling (with replacement) a block of the sampling domain having the same shape and volume as the region, creating a spatial permutation of blocks of sampling locations. When using the resampling methods, the user must choose the window or block size and the conclusion of the test has the potential to change based on the chosen size. Irregularly shaped sampling domains can pose a challenge in using the subsampling methods. For example, for an irregularly shaped sampling domain, many incomplete blocks may complicate the subsampling procedure. We summarize guidelines for choosing the window/block size in Section 5.

Another approach to testing isotropy in the spatial domain is given by [Bowman and Crujeiras \(2013\)](#) who take a more empirical and computationally-intensive approach. Their methods are available in the R software ([R Core Team, 2014](#)) package `sm` ([Bowman and Azzalini, 2014](#)). One caveat of using the `sm` package is that the methods are computationally expensive, even for moderate sample sizes. For example, a test of isotropy on 300 uniformly distributed sampling locations on a  $10 \times 16$  sampling domain took approximately 9.5 minutes where the methods from [Guan et al. \(2004\)](#) took 1.6 seconds using a laptop with 8 GB of memory and a 2 GHz Intel Core i7 processor. Because of the computational costs, we do not consider this method further.

### 3.3 Nonparametric Methods in the Spectral Domain

For gridded sampling locations, nonparametric spectral methods have been developed for testing symmetry ([Scaccia and Martin, 2002, 2005](#); [Lu and Zimmerman, 2005](#)) and stationarity ([Fuentes, 2005](#)), but none are designed with a primary goal of testing isotropy. Due to the difficulties presented by non-gridded sampling locations, historically there have been fewer developments using spectral methods for non-gridded sampling locations than for gridded (or lattice) data, but this is an area that has received more attention recently (see, e.g., [Fuentes, 2007](#); [Matsuda and Yajima, 2009](#); [Bandyopadhyay et al., 2015](#)). Despite the challenges, [Van Hala et al. \(2014\)](#) have proposed a nonparametric, empirical likelihood approach to test isotropy and separability for non-gridded sampling locations.

The primary motivation for using the spectral domain over the spatial domain

are simpler asymptotics in the spectral domain. Unlike estimates of the variogram or covariogram at different spatial lags, estimates of the spectral density at different frequencies via the periodogram are asymptotically independent under certain conditions (Pagano, 1971; Schabenberger and Gotway, 2004, pg. 78,194). Additionally, in practice, tests of symmetry in the spectral domain are generally not subject to as many choices (e.g., spatial lag set, bandwidth, block size) as those in the spatial domain.

Analogous to testing isotropy in the spatial domain by using a finite set of spatial lags, tests of symmetry in the spectral domain typically involve estimating and comparing the spectral density (2.4) at a finite set of the Fourier frequencies. For example, axial symmetry (2.2) of the covariance function implies axial symmetry of the spectral density,  $f(\omega_1, \omega_2) = f(-\omega_1, \omega_2)$ , which can be evaluated by comparing  $I(\omega_1, \omega_2)$  to  $I(-\omega_1, \omega_2)$  at a finite set of frequencies. Similarly, the null hypothesis of isotropy can be approximated by comparing periodogram (2.5) estimates at a set of distinct frequencies with the same norm (Fuentes, 2005). Although most of the current spectral methods are not directly designed to test isotropy, the hypothesis of complete symmetry can be used to reject the assumption of isotropy due to (2.3). However, certain types of anisotropy may not be detected by these tests. For example, a geometrically anisotropic process having the major axis of the ellipses of equicorrelation parallel to the  $x$ -axis is axially symmetric, and the anisotropy wouldn't be detected by a test of axial symmetry.

Scaccia and Martin (2002, 2005) use the periodogram (2.5) to develop a test for axial symmetry. They propose three test statistics that are a function of the periodogram values. The first uses the average of the difference in the log of the periodogram values,  $\log[I(\omega_1, \omega_2)] - \log[I(\omega_1, -\omega_2)]$ . The second and third test statistics use the average of standardized periodogram differences,  $[I(\omega_1, \omega_2) - I(\omega_1, -\omega_2)]/[I(\omega_1, \omega_2) + I(\omega_1, -\omega_2)]$ . These test statistics are shown to asymptotically follow a standard normal or  $t$  distribution via the Central Limit Theorem, and the corresponding distributions are used to obtain a p-value.

Lu and Zimmerman (2005) also use the periodogram as an estimator of the spectral density to test properties of axial and complete symmetry of processes on the integer grid,  $\mathbb{Z}^2$ . They use the asymptotic distribution of the periodogram to construct two potential test statistics. Both test statistics leverage the fact that, under certain conditions and at certain frequencies,

$$(3.5) \quad \frac{2I(\omega_1, \omega_2)}{f(\omega_1, \omega_2)} \xrightarrow[n_1, n_2 \rightarrow \infty]{\text{iid}} \chi_2^2.$$

Under the null hypothesis of axial or complete symmetry, (3.5) implies that ratios of periodogram values at different frequencies follow an  $F(2, 2)$  distribution. The preferred test statistic produces a p-value via a Cramér-von Mises (CvM) goodness of fit test using the appropriate set of periodogram ratios. Because rejecting a hypothesis of axial symmetry implies rejecting a hypothesis of complete symmetry, Lu and Zimmerman (2005) recommend a two-stage procedure for testing complete symmetry. At the first stage, they test the hypothesis of axial symmetry, and if the null hypothesis is not rejected, they test the hypothesis of complete symmetry. To control the overall type-I error rate at  $\alpha$ , the tests at each stage can be performed using a significance level of  $\alpha/2$ .

Leveraging the asymptotic independence of the periodogram at different frequencies, Van Hala et al. (2014) propose a spatial frequency domain empirical

likelihood (SFDEL) approach that can be used for inference about spatial covariance structure. One of the applications of this method is testing isotropy. An advantage of this method over other frequency domain approaches is that it can be used for non-gridded sampling locations. To implement the test, the user must select the set of lags and, because the sampling locations are not gridded, the number and spacing of frequencies. [Van Hala et al. \(2014\)](#) offer some guidelines for these choices based on the simulations and theoretical considerations (e.g., the frequencies need to be asymptotically distant). Once these choices are made, [Van Hala et al. \(2014\)](#) maximize an empirical likelihood under a moment constraint corresponding to isotropy and show that the log-ratio of the constrained and unconstrained maximizer asymptotically follows a  $\chi^2$  distribution. The SFDEL method relies on the asymptotic independence of the periodogram values, and the smallest sample size used in simulations was  $n = 600$ . Thus, it is not clear how the method will perform for smaller sample sizes.

[Fuentes \(2005\)](#) introduces a nonparametric, spatially varying spectral density to represent nonstationary spatial processes. While the method can be used to test the assumption of isotropy, the test requires a large sample size on a fine grid. For this reason and also because the test was primarily designed to test the assumption of stationarity, we do not consider it further.

#### 4. SIMULATION STUDY

We designed a simulation study to compare the empirical size, power, and computational costs for four of the methods. For gridded sampling locations, we compare [Lu and Zimmerman \(2005\)](#)[hereafter, LZ] to [Guan et al. \(2004\)](#)[hereafter denoted as GSC or GSC-g when we are specifically referring to the test when applied to gridded sampling locations]. For uniformly distributed sampling locations we compare [Maity and Sherman \(2012\)](#)[MS] to [Guan et al. \(2004, 2007\)](#)[GSC-u for the method used for uniformly distributed sampling locations].

We performed the tests on the same realizations of the RF. Data are simulated on rectangular grids or rectangular sampling domains because they are more realistic than square domains and simulations on rectangular domains were not previously demonstrated. We simulate Gaussian data with mean zero and exponential covariance functions with no nugget, a sill of one, and effective range values corresponding to short, medium, and long range dependence. We introduce varying degrees of geometric anisotropy via coordinate transformations governed by a rotation parameter  $\theta$  and scaling parameter  $R$  that define the ellipses of equicorrelation (see Figure 5 in the Appendix). The parameter  $\theta$  quantifies the angle between the major axis of the ellipse and the  $x$ -axis (counter-clockwise rotation) while  $R$  gives the ratio of the major and minor axes of the ellipse. We also performed simulations that investigate the effect of the lag set, block size, and bandwidth. Although some simulations are given in the original works, our simulations serve to provide a direct comparison of the effects of changing these values and provide further insight into how to choose them. See the Appendix for additional simulation details and results.

Figures 2 and 3 illustrate a subset of the simulation results comprising empirical size, power, and computational time (full results in Appendix, Tables 5 and 6). These simulations indicate that nonparametric tests for anisotropy have higher power for gridded (Figure 5) than for non-gridded (Figure 6) sampling designs.

Table 3: Test Implementation, part 2. This table continues the list of choices and considerations for implementing a given test. “Samp Size (S/A)” indicates the minimum sample sizes used in simulations (S) and applications (A) provided by the author(s) of the method.

Test Method	Hypothesis Test Implementation		
	Choices	Other Considerations	Samp Size (S/A)
<a href="#">Lu and Zimmerman (2001)</a>	spatial lag set, truncation parameter	optimal truncation parameter	100/112
<a href="#">Guan et al. (2004)</a> gridded design	spatial lag set, window size	optimal window size, edge effects, finite sample adjustment	400/289
<a href="#">Guan et al. (2004)</a> uniform design	spatial lag set, kernel function, bandwidth parameter, window size	optimal bandwidth & window size, edge effects, finite sample adjustment	400/289
<a href="#">Guan et al. (2007)</a> non-uniform design	test statistic	requires gridded sampling locations; designed to test symmetry	500/584
<a href="#">Scaccia and Martin (2002, 2005)</a>			121/–
<a href="#">Lu and Zimmerman (2005)</a>	test statistic	requires gridded sampling locations; two-stage testing procedure, designed to test symmetry; relies on asymptotic independence	100/–
<a href="#">Fuentes (2005)</a>	kernel function, bandwidth parameters, frequency set, spatial knots	requires fine grid; designed to test stationarity	5175/5175
<a href="#">Maity and Sherman (2012)</a>	lag set $\mathbf{A}$ , kernel function, bandwidth parameter, subblock size, number of bootstrap samples	optimal bandwidth & block size	350/584
<a href="#">Bowman and Crujeiras (2013)</a>	bandwidth parameter	computationally intensive	49/148
<a href="#">Van Hala et al. (2014)</a>	lag set, number and spacing of frequencies	optimal number and spacing of frequencies, relies on asymptotic independence	600/–

In both comparisons the methods from [GSC](#) have favorable empirical power over the competitor with a comparable empirical size. As the effective range increases, both empirical size and power tend to increase for the methods from [GSC](#), but they tend to decrease for [MS](#). [GSC-g](#) and [LZ](#) have similar computation time, while [MS](#) is much more computationally expensive than [GSC-u](#). This difference is due to the bootstrapping required by [MS](#).

Unsurprisingly, as the strength of anisotropy increases (measured by  $R$ ), power increases for all the methods. For a geometrically anisotropic process, the major and minor axes of anisotropy are orthogonal. In comparing the effect of the orientation of isotropy ( $\theta$ ) on the methods, it is important to note that when  $\theta = 0$ , the major axis of the ellipse defining the geometric anisotropy is parallel to the  $x$ -axis and corresponds to a spatial process that is axially symmetric but not completely symmetric. When  $\theta = 3\pi/8$  the major axis of the ellipse forms a 67.5-degree angle with the  $x$ -axis, and the spatial process is neither axially nor completely symmetric (see Figure 5 in the Appendix for contours of equal correlation used in the simulation). The original works generally only simulate data from a geometrically anisotropic process with the major axis of anisotropy forming a 45-degree angle with the  $x$ -axis; hence, our simulation study more carefully explores the effect of changing the orientation of geometric anisotropy. The methods from [GSC](#) exhibit higher power when  $\theta = 0$  than when  $\theta = 3\pi/8$ . This is due to the fact that the lag set,  $\mathbf{\Lambda}$ , from (3.2) used for the tests contains a pair of spatial lags that are parallel to the major and minor axes of anisotropy when  $\theta = 0$ , indicating that an informed choice of spatial lags improves the test's ability to detect anisotropy. This same result does not hold for [MS](#). It is unclear whether this behavior is observed because the method uses the covariogram rather than the semivariogram, the GBBB rather than moving window approach for estimating  $\mathbf{\Sigma}$ , or perhaps both. The simulation results indicate that the [LZ](#) test has low empirical power; however, this method was developed to test symmetry properties on square grids, and the choice of a rectangular grid for our simulation study does not allow for a large number of periodogram ordinates for the second stage of the procedure for testing the complete symmetry hypothesis.

Results from simulations that investigate the effects of changing the lag set, the block size, and the bandwidth for non-gridded sampling locations are displayed in Tables 7-9, respectively, in the Appendix. For both [GSC-u](#) and [MS](#), the lag set in (3.2) provided an empirical size close to the nominal level. Using more lags or longer lags decreased the size and power for [GSC-u](#). This may be due to the additional uncertainty induced by estimating the covariance between the semivariance at more lags and the larger variance of semivariance estimates at longer lags. For [MS](#) the longer lags lead to an inflated size and more lags decreased the power. In this case, the GBBB may not be capturing the uncertainty in covariance estimates at longer lags with the chosen block size. The [MS](#) test was not overly sensitive to block size with larger blocks leading to slightly higher power. [MS](#) found that an overly large block size was adverse for test size. For [GSC-u](#) the small and normal sized windows performed at nominal size levels with comparable power while larger windows were detrimental to test size and power. For [GSC-u](#), we find that choosing a large window tends to lead to overestimation of the asymptotic variance-covariance matrix due to fewer blocks being used to re-estimate the semivariance. Finally, the results investigating the bandwidth



selection for [GSC-u](#) indicate that choosing an overly large bandwidth inflates test size while choosing too small a bandwidth deflates test size and power. However, the results also indicate that, for the small sample size, test size and power are less negatively affected when approximating the p-value via the finite sample adjustment.

[Weller \(2015b\)](#) demonstrates applications of several of these methods on two real data sets. The R package `spTest` ([Weller, 2015a](#)) implements the tests in [LZ](#), [GSC](#), and [MS](#) for rectangular grids and sampling regions and is available on the Comprehensive R Archive Network ([CRAN](#)).

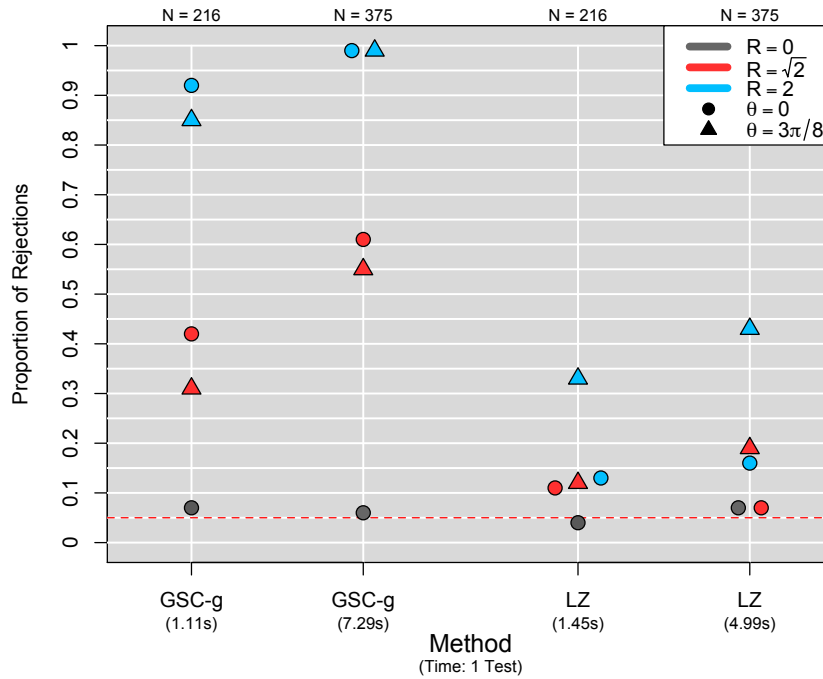


Fig 2: Empirical size and power for [Guan et al. \(2004\)](#) [GSC-g] and [Lu and Zimmerman \(2005\)](#) [LZ] for 500 realizations of a mean 0 GRF with gridded sampling locations using a nominal level of  $\alpha = 0.05$ . Colors and shapes indicate the type of anisotropy. Gray points correspond to the isotropic case. The results correspond to a “medium” effective range. Computational time for each method is also displayed.

## 5. RECOMMENDATIONS

Based on the simulation results we offer recommendations for implementation of nonparametric tests of isotropy. The flow chart in [Figure 1](#) along with [Figure 4](#) summarize the steps in the process. [Tables 1-3](#) compare the tests. [Table 4](#) summarizes the recommendations provided below.

In choosing a nonparametric test for isotropy, the distribution of sampling locations on the sampling domain is perhaps the most important consideration. Data on a grid simplifies estimation because the semivariogram or covariogram



Table 4: General Recommendations for Test Implementation. This table contains a list of general recommendations for test implementation. These guidelines will not apply in all situations and will vary based on a variety of factors including, but not limited to, the sample size, density of sampling locations, and scale of the problem. See additional discussion in Section 5.

		Hypothesis Test Choices			
Test Method	Lag Set <sup>a</sup>	Block Size	Bandwidth	P-value	min. $n$
Guan et al. (2004) gridded design	Length: shorter preferred Orientation: Eqn (3.2) Number: 4 (2 pairs)	$n_b < n^{1/2}$	$n/a$	finite sample adjustment	150
Guan et al. (2004, 2007) uniform design		$n_b \lesssim n^{1/2}$	$0.6 < w < 0.9^b$	finite sample adjustment when $n < 500$ , asymptotic $\chi^2$ when $n \geq 500$	300
Maity and Sherman (2012)		$n_b \gtrsim n^{1/2}$	empirical bandwidth	asymptotic $\chi^2$	300

<sup>a</sup> Prior knowledge, if available, should be used to inform the choice of lags.  
<sup>b</sup> Our simulations suggest these bandwidth values are reasonable when using a Gaussian kernel with truncation parameter of 1.5.

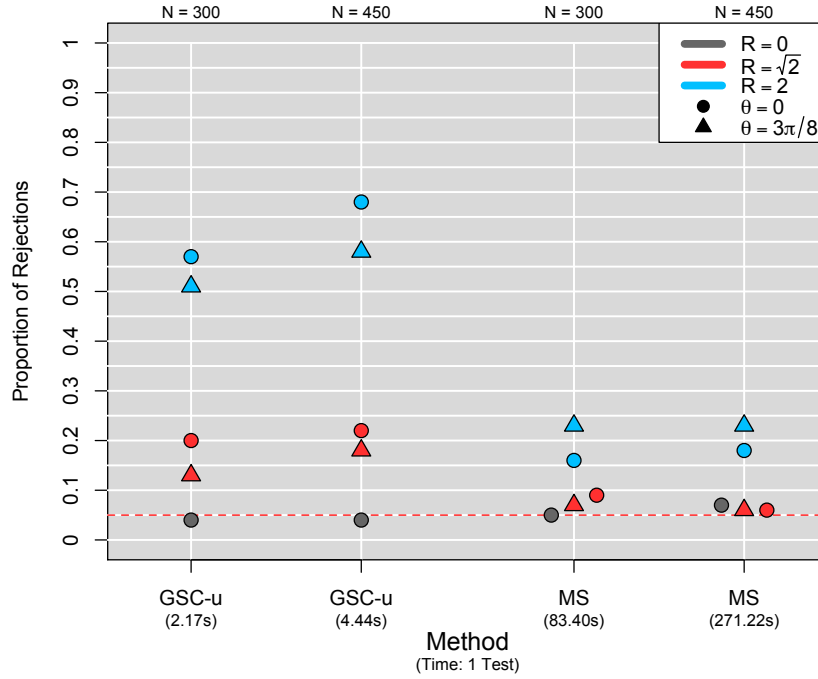


Fig 3: Empirical size and power for Guan et al. (2004) [denoted GU] and Maity and Sherman (2012) [denoted MS] for 200 realizations of a mean 0 GRF with uniformly distributed sampling locations using a nominal level of  $\alpha = 0.05$ . Colors and shapes indicate the type of anisotropy. Gray points correspond to the isotropic case. The results correspond to a “medium” effective range. Computational time for each method is also displayed.

can be estimated at spatial lags that are exactly observed separating pairs of sampling locations. A grid also allows the option of using easily implemented tests in the spectral domain.

Sample size requirements for the asymptotic properties of tests using the spatial domain to approximately hold will depend on the dependence structure of the random field. GSC note that convergence of their test statistic is slow in the case of gridded sampling locations and obtain an approximate p-value via subsampling rather than the asymptotic  $\chi^2$  distribution. Tests using the spectral domain rely on the asymptotic independence of periodogram values, and correlation in finite samples can lead to an inflated test size (LZ). Based on our simulations, we recommend the sample size be at least 150 for gridded sampling locations and at least 300 for non-gridded sampling locations. However, power tends to be low when the sample size is small and/or the anisotropy is weak (Figures 2 and 3).

We focus on implementation of the methods that use the spatial domain for the remainder of this section. We discuss the choice of lags, block size, and bandwidth for the tests in GSC and MS. Due to the large number of choices required to implement the tests (e.g., block size, bandwidth, kernel function, subsampling method), features of the random field (e.g., sill, range), and properties of the

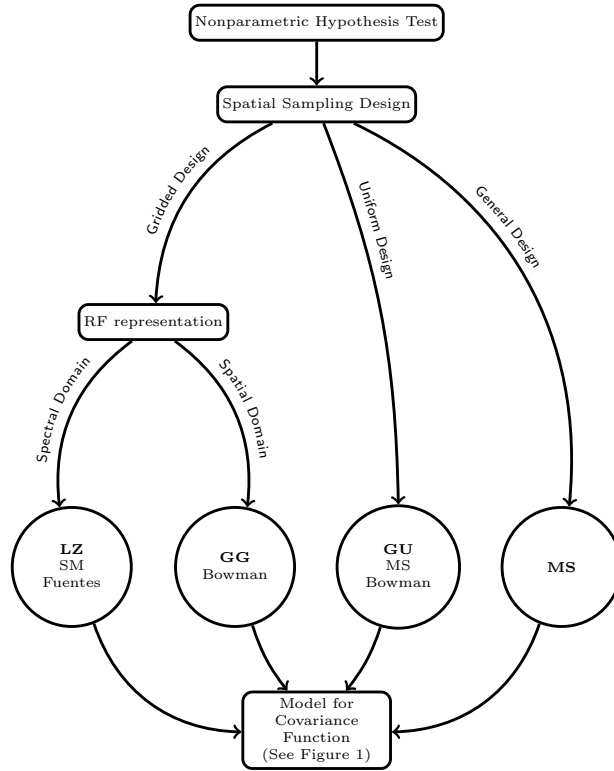


Fig 4: Spatial sampling design considerations for choosing a nonparametric hypothesis test of isotropy. The method we recommended for testing isotropy in each situation is given in bold including LZ = [Lu and Zimmerman \(2005\)](#); SM = [Scaccia and Martin \(2005\)](#); GSC-g = [Guan et al. \(2004\)](#) for gridded sampling locations; GSC-u = [Guan et al. \(2004\)](#) for uniformly distributed sampling locations; MS = [Maity and Sherman \(2012\)](#); GSC-n = [Guan et al. \(2007\)](#) for non-uniform sampling locations.

sampling design (e.g., density of sampling locations, shape of sampling domain), the recommendations we offer will not apply in all situations. The numerous moving parts make it challenging to develop general recommendations, especially when choosing a bandwidth.

When determining the lag set,  $\mathbf{\Lambda}$ , for use in (3.1), the user needs to select

- (a) the norm of the lags (e.g., Euclidean distance),
- (b) the orientation (direction) of the lags, and
- (c) the number of lags.

Regarding (a), short lags are preferred. Estimates of the spatial dependence at large lags may be less reliable than estimates at shorter lags because they are based on a smaller number of pairs of observations and hence more variable. Additionally, empirical and theoretical evidence ([Lu and Zimmerman, 2001](#)) indicates that values of  $\gamma(\cdot)$  in two different directions generally exhibit the largest difference at a lag less than the effective range, the distance beyond which pairs of observations can be assumed to be independent. Finally, there is mathematical support that correctly specifying the covariance function at short lags is

important for spatial prediction (Stein, 1988). Considering (b), if the process is anisotropic, the ideal choice of  $\mathbf{\Lambda}$  and  $\mathbf{A}$  contrasts lags with the same norm but oriented in the direction of weakest and strongest spatial correlation. Typically, the directions of weakest and strongest spatial correlation will be orthogonal and thus, lags contrasted using the  $\mathbf{A}$  matrix should also be orthogonal. Prior information, if available, about the underlying physical/biological process giving rise to the data can also be used to inform the orientation of the lags (Guan et al., 2004). If no prior information about potential anisotropy is available, lags oriented in the same directions as those in (3.2) are a good starting set. In regards to (c), detecting certain types of anisotropy requires a sufficient number of lags but using a large number of lags requires a large number of observations (Guan et al., 2004). As a general guideline, we suggest using four lags to construct two contrasts.

Several tests require selection of a window or block size to estimate the variance-covariance matrix. The moving window from GSC creates overlapping subblocks of data by sliding the window over a grid placed on the region. Each of these subblocks are used to re-estimate the semivariance. The block size from MS defines the size of resampled blocks when implementing the GBBB. The GBBB permutes resampled blocks to create a new realization of the process over the entire domain. Choosing the window size in GSC requires balancing two competing goals. First, the moving window should be large enough to create subblocks that are representative of the dependence structure for the entire RF. Second, the window should be small enough to allow for a sufficient number of subblocks to re-estimate the semivariance, as these values are used to obtain an estimate of the asymptotic variance-covariance. A window that is too large or too small can potentially lead to under- or over-estimation of the asymptotic variance-covariance. For GSC-u, the windows must be large enough to ensure enough pairs of sampling locations are in each subblock to compute an estimate of the semivariance without having to over-smooth. For gridded sampling locations, GSC demonstrate good empirical size and power by using moving windows with size of only  $2 \times 2$ . However, they find slow convergence to the asymptotic  $\chi^2$  distribution, and a p-value is instead computed by approximating the distribution of the test statistic by computing its value for each of the subblocks. Hence, approximating the p-value to two decimal places will require at least 100 subblocks over the sampling region. This may not be possible in practice. For example, a  $12 \times 12$  grid of sampling locations with moving windows of size  $2 \times 2$  results in only 90 subblocks when correcting for edge effects. The challenge of choosing the block size in MS is subject to similar considerations as the window size in GSC. The p-value for both tests will change when performing the test with different window or block sizes, and the user may decide to run the test with different block sizes (e.g., MS). There are a number of works on resampling spatial data to obtain an estimate of the variance of a spatial statistic (e.g., Sherman, 1996; Politis and Sherman, 2001; Lahiri, 2003; Lahiri and Zhu, 2006), but they do not directly consider variance estimation in the case of a nonparametric estimate of the semivariogram/covariogram. Denoting the number of points per block as  $n_b$ , Sherman (1996) proposes choosing the block size such that  $n_b \approx cn^{1/2}$  for a constant,  $c$ , when the spatial dependence does not exhibit a large range. In a number of different applications of spatial subsampling,  $c$  is typically chosen to be between 0.5 and 2 (Politis and Sherman, 2001; Guan

et al., 2004, 2006). Based on our simulations, we find acceptable empirical size and power for **GSC-g** using small windows and approximating the p-value with the finite sample adjustment. Thus, we recommend setting  $n_b < n^{1/2}$  for **GSC-g**. For example, we used windows with size  $3 \times 2$  and  $5 \times 3$  for sampling domains of  $18 \times 12$  and  $25 \times 15$ , respectively. In the case of uniformly distributed sampling locations (see Table 8 in the Appendix), the empirical size and power from **GSC-u** was negatively affected by a large moving window size; hence, we recommend setting  $c = 1$  and choosing  $n_b \lesssim n^{1/2}$ . For the **MS** test, a small block size negatively affected the empirical size and power; thus, we recommend choosing  $n_b \gtrsim n^{1/2}$  for this test.

Between the choices of a lag set, block size, and bandwidth, choosing an appropriate bandwidth to smooth over observed spatial lags for non-gridded sampling locations is the most challenging. For **GSC-u** the user needs to choose the form of the smoothing kernel as well as the bandwidth for both the entire grid and the subblocks while **MS** use an Epanechnikov kernel and empirical bandwidth based on a user-specified tuning parameter. If the selected bandwidth is too large then over-smoothing occurs. In oversmoothing, there is very little filtering of the lag distance and direction. The lack of filtering produces similar estimates of the spatial dependence at lags with different directions and distances. If the selected bandwidth is too small, then there is very little smoothing and estimates of the spatial dependence are based on a small number of pairs of sampling locations and thus highly variable. Considering the aforementioned effects of the bandwidth, the bandwidth should decrease as  $n$  increases under the usual increasing domain asymptotics. For example, simulations (not included) indicated a bandwidth of  $w = 0.65$  maintains nominal size when  $n = 950$ , but leads to deflated test size and power when  $n = 400$  on a smaller domain. García-Soidán et al. (2004), García-Soidán (2007), and Kim and Park (2012) develop theoretically optimal bandwidths for nonparametric semivariogram estimation, but these works are not applicable here because they focus on the isotropic case and require an estimate of the second derivative of the variogram. We have found that the empirical bandwidth used by **MS** tends to produce nominal size (see Table 6). For **GSC-u** we find the most consistent results with a bandwidth in the range of  $0.60 < w < 0.90$  when using a normal kernel truncated at 1.5, but these values will change when a different truncation value or kernel function are employed. For small sample sizes ( $n < 500$ ), our simulations demonstrate that test size and power are less affected by the choice of bandwidth when the p-value is approximated using a finite sample adjustment, indicating poor convergence to the asymptotic  $\chi^2$  distribution. Thus, the user should consider using the finite sample adjustment for non-gridded sampling locations when the sample size is small there are at least 100 subblocks. While it is challenging to choose a bandwidth for **GSC-u** and the p-value of the test is sensitive to this parameter, the method exhibits nominal size and substantially higher power than **MS** when chosen appropriately.

## 6. CONCLUSIONS

There are several important avenues of future research. Methods to more formally characterize the optimal block size and bandwidth parameters for the tests in the spatial domain would enhance the applicability of the tests. The performance of the tests for non-gridded data in Guan et al. (2004) and Maity and

Sherman (2012) are sensitive to these choices and their optimality remains an open question. Zhang et al. (2014) develop a nonparametric method for estimating the asymptotic variance-covariance matrix of statistics derived from spatial data that avoids choosing tuning parameters which could simplify test implementation. A second area of future work is further development of nonparametric tests of isotropy for gridded and non-gridded data in the spectral domain. A third area of further investigation is to compare nonparametric to parametric methods for testing isotropy, e.g., Scaccia and Martin (2011). A final area of future work is development of a formal definition and more careful quantification of power of the tests. For example, the degree of geometric anisotropy could be quantified using different characteristics of the covariance function, including the ratio of the major and minor axes of the ellipse, degree of rotation of the ellipse from the coordinate axes, and range of the process. Furthermore, it is important to consider the effects of density and design of sampling locations, sample size, and the amount of noise (nugget and sill) in the observations on a test's ability to detect anisotropy.

There is a volume of work on tests for isotropy in other areas of spatial statistics. Methods for detecting anisotropy in spatial point process data have been developed, e.g., Schabenberger and Gotway (2004, pg. 200-205), Guan (2003), Guan et al. (2006), and Nicolis et al. (2010). For multivariate spatial data, Jona-Lasinio (2001) proposes a test for isotropy. Gneiting et al. (2007) provide a review of potential second order assumptions and models for spatiotemporal geostatistical data, and a number of tests for second order properties of spatiotemporal data have been developed, e.g., Fuentes (2006), Li et al. (2007), Park and Fuentes (2008), Shao and Li (2009), Jun and Genton (2012). Li et al. (2008a) construct a test of the covariance structure for multivariate spatiotemporal data. Tests for isotropy have also been developed in the computer science literature (e.g., Molina and Feito, 2002; Chorti and Hristopulos, 2008; Spiliopoulos et al., 2011; Thon et al., 2015).

Appropriately specifying the second order properties of the random field is an important step in modeling spatial data, and a number of models have been developed to capture anisotropy in spatial processes. Graphical tools, such as directional sample semivariograms, are commonly used to evaluate the assumption of isotropy, but these diagnostics can be misleading and open to subjective interpretation. We have presented and reviewed a number of procedures that can be used to more objectively test hypotheses of isotropy and symmetry without assuming a parametric form for the covariance function. These tests may be helpful for a novice user deciding on an appropriate spatial model. In abandoning parametric assumptions, these hypothesis testing procedures are subject and sensitive to choices regarding smoothing parameters, subsampling procedures, and finite sample adjustments. The test that is most appropriate for a set of data will largely depend on the sampling design. Additionally, there are trade-offs between the empirical power demonstrated by the tests and the number of choices user must make to implement the tests (e.g., between Guan et al. (2004) and Maity and Sherman (2012)). We have offered recommendations regarding the various choices of method and their implementation and have made the tests available in the `spTest` software. Because of the sensitivity of the tests to the various choices, we believe that graphical techniques and nonparametric hypothesis tests should

be used in a complementary role. Graphical techniques can provide an initial indication of isotropy properties and inform sensible choices for a hypothesis test, e.g., in choosing the spatial lag set, while hypothesis tests can affirm intuition about graphical techniques.

## REFERENCES

- Baczkowski, A. (1990). A test of spatial isotropy. In *Compstat*, pages 277–282. Springer.
- Baczkowski, A. and Mardia, K. (1987). Approximate lognormality of the sample semi-variogram under a gaussian process. *Communications in Statistics-Simulation and Computation*, 16(2):571–585.
- Baczkowski, A. and Mardia, K. (1990). A test of spatial symmetry with general application. *Communications in Statistics-Theory and Methods*, 19(2):555–572.
- Bandyopadhyay, S., Lahiri, S. N., Nordman, D. J., et al. (2015). A frequency domain empirical likelihood method for irregularly spaced spatial data. *The Annals of Statistics*, 43(2):519–545.
- Banerjee, S., Carlin, B. P., and Gelfand, A. E. (2014). *Hierarchical modeling and analysis for spatial data*. CRC Press.
- Borgman, L. and Chao, L. (1994). Estimation of a multidimensional covariance function in case of anisotropy. *Mathematical geology*, 26(2):161–179.
- Bowman, A. W. and Azzalini, A. (2014). *R package sm: nonparametric smoothing methods (version 2.2-5.4)*. University of Glasgow, UK and Università di Padova, Italia.
- Bowman, A. W. and Crujeiras, R. M. (2013). Inference for variograms. *Computational Statistics & Data Analysis*, 66:19–31.
- Cabana, E. (1987). Affine processes: a test of isotropy based on level sets. *SIAM Journal on Applied Mathematics*, 47(4):886–891.
- Chorti, A. and Hristopulos, D. T. (2008). Nonparametric identification of anisotropic (elliptic) correlations in spatially distributed data sets. *Signal Processing, IEEE Transactions on*, 56(10):4738–4751.
- Cressie, N. (1993). *Statistics for Spatial Data: Wiley Series in Probability and Statistics*. Wiley-Interscience New York.
- Ecker, M. D. and Gelfand, A. E. (1999). Bayesian modeling and inference for geometrically anisotropic spatial data. *Mathematical Geology*, 31(1):67–83.
- Ecker, M. D. and Gelfand, A. E. (2003). Spatial modeling and prediction under stationary non-geometric range anisotropy. *Environmental and Ecological Statistics*, 10(2):165–178.
- Fuentes, M. (2005). A formal test for nonstationarity of spatial stochastic processes. *Journal of Multivariate Analysis*, 96(1):30–54.
- Fuentes, M. (2006). Testing for separability of spatial-temporal covariance functions. *Journal of statistical planning and inference*, 136(2):447–466.
- Fuentes, M. (2007). Approximate likelihood for large irregularly spaced spatial data. *Journal of the American Statistical Association*, 102(477):321–331.
- Fuentes, M. (2013). Spectral methods. *Wiley StatsRef: Statistics Reference Online*.
- Fuentes, M. and Reich, B. (2010). Spectral domain. *Handbook of Spatial Statistics*, pages 57–77.
- García-Soidán, P. (2007). Asymptotic normality of the Nadaraya–Watson semivariogram estimators. *Test*, 16(3):479–503.
- García-Soidán, P. H., Febrero-Bande, M., and González-Manteiga, W. (2004). Nonparametric kernel estimation of an isotropic variogram. *Journal of Statistical Planning and Inference*, 121(1):65–92.
- Gneiting, T., Genton, M., and Guttorp, P. (2007). Geostatistical space-time models, stationarity, separability and full symmetry. *Statistical Methods for Spatio-Temporal Systems*, pages 151–175.
- Guan, Y., Sherman, M., and Calvin, J. A. (2004). A nonparametric test for spatial isotropy using subsampling. *Journal of the American Statistical Association*, 99(467):810–821.
- Guan, Y., Sherman, M., and Calvin, J. A. (2006). Assessing isotropy for spatial point processes. *Biometrics*, 62(1):119–125.
- Guan, Y., Sherman, M., and Calvin, J. A. (2007). On asymptotic properties of the mark variogram estimator of a marked point process. *Journal of statistical planning and inference*, 137(1):148–161.
- Guan, Y. T. (2003). *Nonparametric methods of assessing spatial isotropy*. PhD thesis, Texas A&M University.



- Hall, P. and Patil, P. (1994). Properties of nonparametric estimators of autocovariance for stationary random fields. *Probability Theory and Related Fields*, 99(3):399–424.
- Haskard, K. A. (2007). *An anisotropic Matérn spatial covariance model: REML estimation and properties*. PhD thesis, University of Adelaide.
- Irvine, K. M., Gitelman, A. I., and Hoeting, J. A. (2007). Spatial designs and properties of spatial correlation: effects on covariance estimation. *Journal of agricultural, biological, and environmental statistics*, 12(4):450–469.
- Isaaks, E. H. and Srivastava, R. M. (1989). *Applied geostatistics*, volume 2. Oxford University Press New York.
- Jona-Lasinio, G. (2001). Modeling and exploring multivariate spatial variation: A test procedure for isotropy of multivariate spatial data. *Journal of Multivariate Analysis*, 77(2):295–317.
- Journel, A. G. and Huijbregts, C. J. (1978). *Mining geostatistics*. Academic press.
- Jun, M. and Genton, M. G. (2012). A test for stationarity of spatio-temporal random fields on planar and spherical domains. *Statistica Sinica*, 22(4):1737.
- Kim, T. Y. and Park, J.-S. (2012). On nonparametric variogram estimation. *Journal of the Korean Statistical Society*, 41(3):399–413.
- Lahiri, S. and Zhu, J. (2006). Resampling methods for spatial regression models under a class of stochastic designs. *The Annals of Statistics*, 34(4):1774–1813.
- Lahiri, S. N. (2003). *Resampling methods for dependent data*. Springer Science & Business Media.
- Li, B., Genton, M. G., and Sherman, M. (2007). A nonparametric assessment of properties of space-time covariance functions. *Journal of the American Statistical Association*, 102(478):736–744.
- Li, B., Genton, M. G., and Sherman, M. (2008a). Testing the covariance structure of multivariate random fields. *Biometrika*, 95(4):813–829.
- Li, B., Genton, M. G., Sherman, M., et al. (2008b). On the asymptotic joint distribution of sample space-time covariance estimators. *Bernoulli*, 14(1):228–248.
- Lu, H. and Zimmerman, D. (2001). Testing for isotropy and other directional symmetry properties of spatial correlation. *preprint*.
- Lu, H.-C. (1994). *On the distributions of the sample covariogram and semivariogram and their use in testing for isotropy*. PhD thesis, University of Iowa.
- Lu, N. and Zimmerman, D. L. (2005). Testing for directional symmetry in spatial dependence using the periodogram. *Journal of Statistical Planning and Inference*, 129(1):369–385.
- Maity, A. and Sherman, M. (2012). Testing for spatial isotropy under general designs. *Journal of statistical planning and inference*, 142(5):1081–1091.
- Matheron, G. (1961). Precision of exploring a stratified formation by boreholes with rigid spacing-application to a bauxite deposit. In *International Symposium of Mining Research, University of Missouri*, volume 1, pages 407–22.
- Matheron, G. (1962). *Traité de géostatistique appliquée*. Editions Technip.
- Matsuda, Y. and Yajima, Y. (2009). Fourier analysis of irregularly spaced data on rd. *Journal of the Royal Statistical Society: Series B (Statistical Methodology)*, 71(1):191–217.
- Modjeska, J. S. and Rawlings, J. (1983). Spatial correlation analysis of uniformity data. *Biometrics*, pages 373–384.
- Molina, A. and Feito, F. R. (2002). A method for testing anisotropy and quantifying its direction in digital images. *Computers & Graphics*, 26(5):771–784.
- Nadaraya, E. A. (1964). On estimating regression. *Theory of Probability & Its Applications*, 9(1):141–142.
- Nicolis, O., Mateu, J., and DErcole, R. (2010). Testing for anisotropy in spatial point processes. In *Proceedings of the Fifth International Workshop on Spatio-Temporal Modelling*, pages 1990–2010.
- Pagano, M. (1971). Some asymptotic properties of a two-dimensional periodogram. *Journal of Applied Probability*, 8(4):841–847.
- Park, M. S. and Fuentes, M. (2008). Testing lack of symmetry in spatial-temporal processes. *Journal of statistical planning and inference*, 138(10):2847–2866.
- Politis, D. N. and Sherman, M. (2001). Moment estimation for statistics from marked point processes. *Journal of the Royal Statistical Society: Series B (Statistical Methodology)*, 63(2):261–275.
- Possolo, A. (1991). Subsampling a random field. *Lecture Notes-Monograph Series*, pages 286–294.

- Priestley, M. and Rao, T. S. (1969). A test for non-stationarity of time-series. *Journal of the Royal Statistical Society. Series B (Methodological)*, pages 140–149.
- Priestley, M. B. (1981). *Spectral analysis and time series*. Academic press.
- R Core Team (2014). *R: A Language and Environment for Statistical Computing*. R Foundation for Statistical Computing, Vienna, Austria.
- Scaccia, L. and Martin, R. (2002). Testing for simplification in spatial models. In *Compstat*, pages 581–586. Springer.
- Scaccia, L. and Martin, R. (2005). Testing axial symmetry and separability of lattice processes. *Journal of Statistical Planning and Inference*, 131(1):19–39.
- Scaccia, L. and Martin, R. (2011). Model-based tests for simplification of lattice processes. *Journal of Statistical Computation and Simulation*, 81(1):89–107.
- Schabenberger, O. and Gotway, C. A. (2004). *Statistical methods for spatial data analysis*. CRC Press.
- Shao, X. and Li, B. (2009). A tuning parameter free test for properties of space–time covariance functions. *Journal of Statistical Planning and Inference*, 139(12):4031–4038.
- Sherman, M. (1996). Variance estimation for statistics computed from spatial lattice data. *Journal of the Royal Statistical Society. Series B (Methodological)*, pages 509–523.
- Sherman, M. (2011). *Spatial statistics and spatio-temporal data: covariance functions and directional properties*. John Wiley & Sons.
- Spiliopoulos, I., Hristopulos, D. T., Petrakis, M., and Chorti, A. (2011). A multigrid method for the estimation of geometric anisotropy in environmental data from sensor networks. *Computers & Geosciences*, 37(3):320–330.
- Stein, M. L. (1988). Asymptotically efficient prediction of a random field with a misspecified covariance function. *The Annals of Statistics*, 16(1):55–63.
- Stein, M. L., Chi, Z., and Welty, L. J. (2004). Approximating likelihoods for large spatial data sets. *Journal of the Royal Statistical Society: Series B (Statistical Methodology)*, 66(2):275–296.
- Thon, K., Geilhufe, M., and Percival, D. B. (2015). A multiscale wavelet-based test for isotropy of random fields on a regular lattice. *Image Processing, IEEE Transactions on*, 24(2):694–708.
- Van Hala, M., Bandyopadhyay, S., Lahiri, S. N., and Nordman, D. J. (2014). A frequency domain empirical likelihood for estimation and testing of spatial covariance structure. *preprint*.
- Vecchia, A. V. (1988). Estimation and model identification for continuous spatial processes. *Journal of the Royal Statistical Society. Series B (Methodological)*, pages 297–312.
- Watson, G. S. (1964). Smooth regression analysis. *Sankhyā: The Indian Journal of Statistics, Series A*, pages 359–372.
- Weller, Z. (2015a). *spTest: Nonparametric Hypothesis Tests of Isotropy and Symmetry*. R package version 0.2.2.
- Weller, Z. D. (2015b). *spTest: an R package implementing nonparametric tests of isotropy. submitted to Journal of Statistical Software, available on arXiv*.
- Zhang, X., Li, B., and Shao, X. (2014). Self-normalization for spatial data. *Scandinavian Journal of Statistics*, 41(2):311–324.
- Zimmerman, D. L. (1993). Another look at anisotropy in geostatistics. *Mathematical Geology*, 25(4):453–470.

## APPENDIX

## SIMULATION STUDY DETAILS AND FURTHER RESULTS

We define the isotropic exponential covariance function as

$$(6.1) \quad C(h) = \begin{cases} \sigma^2 \exp(-\phi h) & \text{if } h > 0, \\ \tau^2 + \sigma^2 & \text{otherwise} \end{cases}$$

where  $h = \|\mathbf{s}_i - \mathbf{s}_j\|$  is the distance between sites  $\mathbf{s}_i$  and  $\mathbf{s}_j$  (Irvine et al., 2007). The corresponding semivariogram is  $\gamma(h) = (\tau^2 + \sigma^2) - \sigma^2 \exp(-\phi h)$ , where  $\tau^2$  is the nugget,  $\tau^2 + \sigma^2$  is the sill, and the effective range,  $\xi$ , the distance beyond which the correlation between observations is less than 0.05, is

$$\xi = \frac{-1}{\phi} \log \left( 0.05 \frac{\tau^2 + \sigma^2}{\sigma^2} \right).$$

Simulations in Section 4 were performed using the exponential covariance function (6.1) with a partial sill,  $\sigma^2$ , of 1 and no nugget,  $\tau^2 = 0$ . We also performed simulations using different nugget values (results not included). As expected, introducing a nugget had an adverse effect on empirical test size and power. For the no nugget simulations, effective ranges,  $\xi$ , for isotropic processes were chosen to be 3, 6, and 12 corresponding to short, medium, and long range dependence. Geometric anisotropy was introduced by transforming the sampling locations according to a scaling parameter,  $R$ , and a rotation parameter,  $\theta$ . Given an  $(R, \theta)$  pair, the coordinates  $(x, y)$  are transformed to the “anisotropic” coordinates,  $(x_a, y_a)$  via

$$(x_a, y_a) = (x, y) \begin{bmatrix} \cos \theta & \sin \theta \\ -\sin \theta & \cos \theta \end{bmatrix} \begin{bmatrix} 1 & 0 \\ 0 & \frac{1}{R} \end{bmatrix}.$$

A realization from the anisotropic process is then created by simulating using the distance matrix from the transformed coordinates and placing the observed values at their corresponding untransformed sampling locations. Figure 5 shows the isotropic exponential correlogram corresponding to  $\tau^2 = 1$  and  $\xi = 6$  and contours of equicorrelation corresponding to the  $(R, \theta)$  values used in the simulation study. Note that a larger value of  $R$  corresponds to a more anisotropic process.

For the simulations comparing the GSC-g and LZ (Lu and Zimmerman, 2005) tests in Table 5, data were simulated on a subset of the integer grid,  $\mathbb{Z}^2$ . The p-values for the GG test were approximated using a finite sample statistic (Guan et al., 2004), and we used the lag set in (3.2) and  $\mathbf{A}$  matrix in (3.3). For the results involving the LZ test, a test of complete symmetry was performed as an approximation to the null hypothesis of isotropy. The p-values for the LZ test were obtained using the CvM\* statistic. A nominal level of  $\alpha = 0.05$  was maintained by first testing reflection symmetry at  $\alpha = 0.025$  then testing complete symmetry at  $\alpha = 0.025$  if the hypothesis of reflection symmetry was not rejected. For the GG test, the moving window dimensions were  $3 \times 2$  (width, height) and  $5 \times 3$  for the parent grids of  $18 \times 12$  and  $25 \times 15$ , respectively.

For the simulations in Table 6 comparing the GU (Guan et al., 2004) and MS (Maity and Sherman, 2012) tests, data were simulated at random, uniformly distributed sampling locations on  $10 \times 16$  and  $10 \times 20$  sampling domains. The lag set,  $\mathbf{A}$ , used for both tests is given in (3.2) with  $\mathbf{A}$  matrix (3.3), and the p-values for both methods were obtained using the asymptotic  $\chi^2_2$  distribution. For

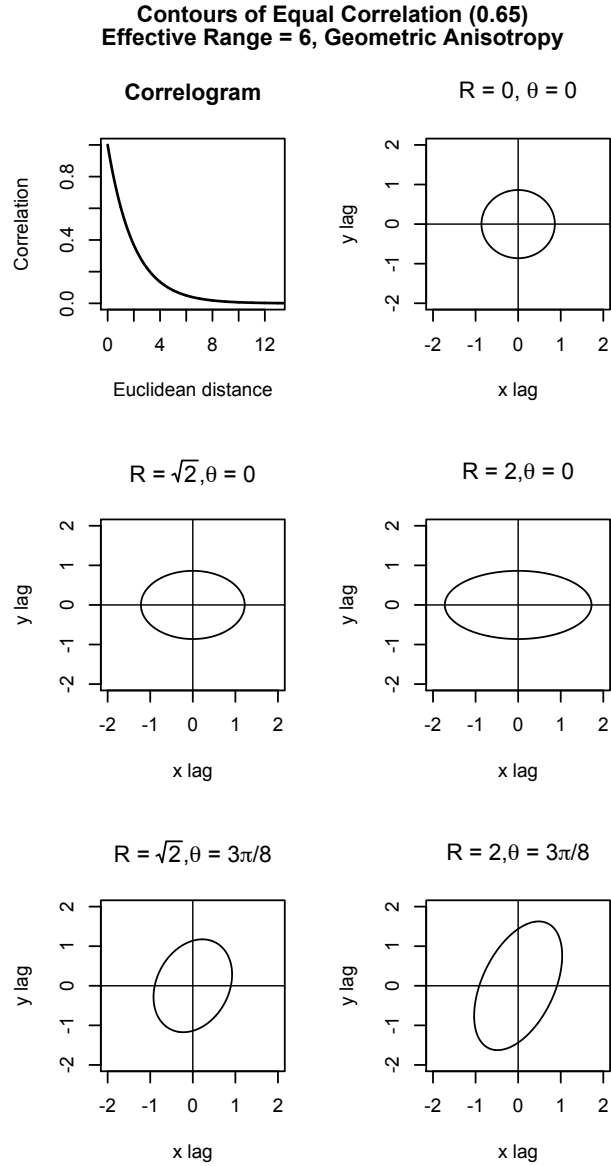


Fig 5: Correlogram and contours of equal correlation for the covariance models used in the simulation study.

semivariogram estimates in GU, we use independent (product) Gaussian (normal) kernels with a truncation parameter of 1.5. The bandwidth for the Gaussian kernel for smoothing over lags on the entire field and on moving windows was chosen as  $w = 0.75$ . We used the empirical bandwidth and the product Epanechnikov kernel given in [Maity and Sherman \(2012\)](#) to implement the MS test. For both tests, a grid with spacing of 1 was laid on the sampling region. Using this grid, the moving window dimensions for the GU test were  $4 \times 2$  and the block size for the MS test were  $4 \times 2$ . For the MS test,  $B = 100$  resamples using the GBBB were used to estimate the asymptotic variance-covariance matrix.

For the results in Tables 7 - 9, we simulated mean 0, Gaussian RFs with exponential covariance function with no nugget, a sill of one, and medium effective range ( $\xi = 6$ ). Sampling locations were generated randomly and uniformly over a  $16 \times 10$  sampling domain. We use the lag set and  $\mathbf{A}$  matrix from 3.2 and 3.3, respectively, unless otherwise noted. All tests were performed using a nominal level of  $\alpha = 0.05$ . For the GU tests, we use product Gaussian kernels with a truncation parameter of 1.5. For the MS tests, we use the default product Epanechnikov kernels with empirical bandwidth specified in [Maity and Sherman \(2012\)](#).

The simulation results in Table 7 demonstrate the effects of changing the set of lags for the GU and MS tests. For these simulations, the lag set labeled “normal” corresponds to the lag set given in (3.2). The lag set labeled “long” represents the lags in (3.2) multiplied by 2.5. Finally, the lag set labeled “more” stands for the lags in (3.2) with the additional pair of lags  $\{\mathbf{h}_5 = (1.132, 0.469), \mathbf{h}_6 = (-0.469, 1.132)\}$ . The lags  $\mathbf{h}_5$  and  $\mathbf{h}_6$  are a pair of lags the create approximate  $22.5^\circ$  and  $112.5^\circ$  angles, respectively, with the  $x$ -axis (counter-clock wise rotation) and have Euclidean length of approximately 1.22. These were chosen to supplement the lag pairs  $(\mathbf{h}_1, \mathbf{h}_2)$  which have unit length and create  $0^\circ$  and  $90^\circ$  angles with the  $x$ -axis and  $(\mathbf{h}_3, \mathbf{h}_4)$  which have length  $\sqrt{2} \approx 1.41$  and create  $45^\circ$  and  $135^\circ$  angles with the  $x$ -axis. The lag sets are plotted in Figure 6. The  $\mathbf{A}$  matrix for the “more” lagset was constructed as in (3.3), where orthogonal lags are contrasted. The p-values were calculated using the asymptotic  $\chi^2$  distribution with degrees of freedom based on the number of pairs of lags contrasted. For the GU method, we used a bandwidth of 0.75. The moving window dimensions were  $4 \times 2$ . For the MS method, we chose block dimensions of  $4 \times 2$  and used  $B = 75$  resamples using the GBBB to estimate the asymptotic variance-covariance matrix. Table 8 demonstrates the effects of changing the block size for the GU and MS tests. For these simulations, the labels “small”, “normal”, and “large” correspond to moving windows/blocks of size  $3 \times 2$ ,  $4 \times 2$ , and  $5 \times 3$ , respectively. Because we simulated  $n = 300$  uniformly distributed sampling locations on a  $16 \times 10$  domain, we expect 1.875 sampling locations per unit area. Thus, we expect  $n_b = 11.3, 15$ , and 28.1 points per block for the small, normal, and large block sizes, respectively. We find that the methods tend to have nominal size when  $n_b \approx n^{1/2} = 17.3$ . For both tests, we used the lags in (3.2), and the blocks are defined by a grid with spacing 0.5 placed on the sampling region (i.e., a  $4 \times 2$  window is achieved by setting the window dimensions to  $8 \times 4$  in the `spTest` software). We performed the tests using a nominal level of  $\alpha = 0.05$ , and the p-values were calculated using the asymptotic  $\chi^2$  distribution. For the GU method, we used a bandwidth of 0.75. For the MS method, we used  $B = 100$  resamples using the GBBB to estimate the asymptotic variance-covariance matrix. Finally, Table 9 demonstrates

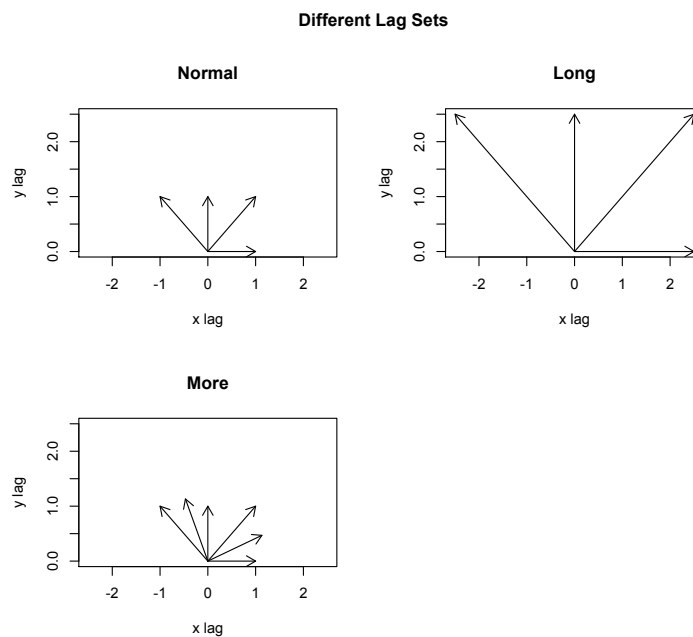


Fig 6: The lag sets used for the simulations in Table 7.

the effects of changing the bandwidth for the GU test. We use bandwidths of  $w = 0.65, 0.75$ , and  $0.85$ . The p-values are calculated using both the asymptotic  $\chi^2$  distribution and using a finite sample adjustment similar to the one used by [Guan et al. \(2004\)](#) for gridded sampling locations.

TABLE 5

Empirical size and power for *Guan et al. (2004)* [denoted GG] and *Lu and Zimmerman (2005)* [denoted LZ] for 500 realizations of a mean 0 GRF with gridded sampling locations using a nominal level of  $\alpha = 0.05$ . Computational time for each method is also included.

(a) Sample size of  $n = 216$  gridded sampling locations.

18 cols $\times$ 12 rows grid					
			effective range		
$R$	$\theta$	Method	3	6	12
0	0	GG	0.05	0.07	0.05
		LZ	0.04	0.04	0.08
$\sqrt{2}$	0	GG	0.32	0.42	0.43
		LZ	0.06	0.11	0.12
2	0	GG	0.91	0.92	0.94
		LZ	0.14	0.13	0.15
$\sqrt{2}$	$\frac{3\pi}{8}$	GG	0.27	0.31	0.34
		LZ	0.14	0.12	0.13
2	$\frac{3\pi}{8}$	GG	0.77	0.85	0.86
		LZ	0.29	0.33	0.33
Computational Time for 1 Test					
GG			1.11 seconds		
LZ			1.45 seconds		

(b) Sample size of  $n = 375$  gridded sampling locations.

25 cols $\times$ 15 rows grid					
			effective range		
$R$	$\theta$	Method	3	6	12
0	0	GG	0.05	0.06	0.07
		LZ	0.06	0.07	0.07
$\sqrt{2}$	0	GG	0.63	0.61	0.69
		LZ	0.07	0.09	0.10
2	0	GG	0.98	0.99	0.99
		LZ	0.14	0.16	0.15
$\sqrt{2}$	$\frac{3\pi}{8}$	GG	0.47	0.55	0.55
		LZ	0.16	0.19	0.18
2	$\frac{3\pi}{8}$	GG	0.97	0.99	0.98
		LZ	0.37	0.43	0.45
Computational Time for 1 Test					
GG			7.29 seconds		
LZ			4.99 seconds		



TABLE 6

Empirical size and power for *Guan et al. (2004)* [denoted GU] and *Maity and Sherman (2012)* [denoted MS] for 200 realizations of a mean 0 GRF with uniformly distributed sampling locations using a nominal level of  $\alpha = 0.05$ . Computational time for each method is also included.

(a) Sample size of  $n = 300$  uniformly distributed sampling locations.

10 height $\times$ 16 width domain					
			effective range		
$R$	$\theta$	Method	3	6	12
0	0	GU	0.02	0.04	0.05
		MS	0.04	0.05	0.04
$\sqrt{2}$	0	GU	0.15	0.20	0.27
		MS	0.10	0.09	0.08
2	0	GU	0.43	0.57	0.62
		MS	0.21	0.16	0.15
$\sqrt{2}$	$\frac{3\pi}{8}$	GU	0.12	0.13	0.16
		MS	0.08	0.07	0.04
2	$\frac{3\pi}{8}$	GU	0.37	0.51	0.51
		MS	0.27	0.23	0.21
Computational Time for 1 Test					
GU			2.17 seconds		
MS			83.40 seconds		

(b) Sample size of  $n = 450$  uniformly distributed sampling locations.

10 height $\times$ 20 width domain					
			effective range		
$R$	$\theta$	Method	3	6	12
0	0	GU	0.00	0.04	0.05
		MS	0.05	0.07	0.03
$\sqrt{2}$	0	GU	0.15	0.22	0.23
		MS	0.07	0.06	0.07
2	0	GU	0.57	0.68	0.75
		MS	0.32	0.18	0.14
$\sqrt{2}$	$\frac{3\pi}{8}$	GU	0.09	0.18	0.21
		MS	0.12	0.06	0.08
2	$\frac{3\pi}{8}$	GU	0.55	0.58	0.65
		MS	0.37	0.23	0.21
Computational Time for 1 Test					
GU				4.44 seconds	
MS				162.35 seconds	

TABLE 7

Effects of changing the lag set. Empirical size and power for *Guan et al. (2004)* [denoted GU] and *Maity and Sherman (2012)* [MS] for 100 realizations of a mean 0 GRF with  $n = 400$  uniformly distributed sampling locations. The label “normal” corresponds to the lag set in (3.2), while “long” represents using longer lags, and “more” denotes using more lags (see Figure 6).

16 width $\times$ 10 height domain					
			Lag Set		
$R$	$\theta$	Method	normal	long	more
0	0	GU	0.02	0.00	0.01
		MS	0.03	0.14	0.03
$\sqrt{2}$	$\frac{3\pi}{8}$	GU	0.19	0.07	0.16
		MS	0.11	0.24	0.07
2	$\frac{3\pi}{8}$	GU	0.56	0.17	0.40
		MS	0.27	0.33	0.21

TABLE 8

Effects of changing the window/block size. Empirical size and power for [Guan et al. \(2004\)](#) [denoted GU] and [Maity and Sherman \(2012\)](#) [MS] for 200 realizations of a mean 0 GRF with  $n = 300$  uniformly distributed sampling locations. The label “normal” corresponds to the window/block size of  $4 \times 2$ , while “small” represents using a smaller window, and “large” denotes using a larger window.

16 width $\times$ 10 height domain					
			Window/Block Size		
$R$	$\theta$	Method	small	normal	large
0	0	GU	0.06	0.04	0.01
		MS	0.03	0.04	0.02
$\sqrt{2}$	0	GU	0.17	0.17	0.08
		MS	0.06	0.09	0.09
2	0	GU	0.56	0.53	0.22
		MS	0.17	0.17	0.18

TABLE 9

Effects of changing bandwidth. Empirical size and power for [Guan et al. \(2004\)](#) [denoted GU] for 100 realizations of a mean 0 GRF with  $n = 400$  uniformly distributed sampling locations using a nominal level of  $\alpha = 0.05$ .

(a) P-value: asymptotic  $\chi^2$  distribution

16 width $\times$ 10 height domain					
			Effective Range		
$R$	$\theta$	Bandwidth	3	6	12
0	0	0.65	0.00	0.00	0.00
		0.75	0.03	0.06	0.04
		0.85	0.06	0.11	0.16
$\sqrt{2}$	$\frac{3\pi}{8}$	0.65	0.01	0.01	0.08
		0.75	0.08	0.14	0.24
		0.85	0.14	0.27	0.35
2	$\frac{3\pi}{8}$	0.65	0.21	0.22	0.25
		0.75	0.50	0.54	0.67
		0.85	0.70	0.73	0.81

(b) P-value: finite sample

16 width $\times$ 10 height domain					
			Effective Range		
$R$	$\theta$	Bandwidth	3	6	12
0	0	0.65	0.02	0.03	0.02
		0.75	0.03	0.06	0.06
		0.85	0.07	0.10	0.09
$\sqrt{2}$	$\frac{3\pi}{8}$	0.65	0.05	0.06	0.20
		0.75	0.09	0.18	0.29
		0.85	0.11	0.24	0.31
2	$\frac{3\pi}{8}$	0.65	0.37	0.38	0.53
		0.75	0.55	0.58	0.69
		0.85	0.63	0.64	0.76